Drag Measurements on a Modified Prolate Spheroid Using a Magnetic Suspension and Balance System

David A. Dress*
NASA Langley Research Center, Hampton, Virginia 23665-5225

Low-speed wind-tunnel drag-force measurements were taken on a modified prolate spheroid free of support interference. This body was tested at zero incidence in the NASA Langley 13-in. Magnetic Suspension and Balance System (MSBS). This shape was one of two bodies tested to determine the drag-force measuring capabilities of the 13-in. MSBS. In addition, support interference on this shape at zero incidence was quantified by using a dummy sting. The drag-force calibrations and wind-on repeatability data let us assess the drag-force measuring capabilities of the 13-in. MSBS. Comparisons with and without the sting showed differences in the drag coefficients with the dummy sting case resulting in lower drag coefficients. Other studies included the effects of fixing transition and surface-flow visualization using oil flow. In addition, the drag coefficient data from this study are compared with data from several other sources.

Nomenclature

C_D = drag coefficient
D = drag force, g_f
d = model diameter, in.
I = electromagnet current, A
L = model length, in.
M = freestream Mach number
R = Reynolds number
x = body abscissa, in.

Subscripts

L = based on model length
wet = based on wetted surface area

Introduction

SUPPORT interference is a serious problem in testing models in wind tunnels.[1,2] Using a magnetic suspension and balance system (MSBS) is the only way to eliminate completely support interference. With the elimination of the support, not only will the flow distortion produced by the sting be eliminated, but many other advantages accrue such as 1) elimination of model modifications to accommodate the sting, 2) ease of model movement for dynamic testing, 3) fast, efficient testing at any attitude, and 4) improvement in productivity due to elimination of stings and struts.

The French at the Office National d'Etudes et de Recherches Aerospatiales first demonstrated a wind-tunnel MSBS in the mid-1950s.[3] Since that time, considerable research efforts have been devoted to MSBS and many improvements have been made. Reference 4 is an extensive bibliography on magnetic suspension and balance systems. During the 1980s, much of the MSBS work at NASA Langley was centered around using and improving the 13-in. MSBS. This sytem has evolved from another MSBS built at the Arnold Engineering Development Center (AEDC) in the early 1960s.[5] Most of the original hardware from the AEDC system has been replaced. For example, the analog control system was replaced with a digital controller using a minicomputer.

Recently, MSBS research at NASA Langley has been aimed at obtaining accurate drag data on various shapes at zero incidence.[6-8] As part of this effort, low-speed wind-tunnel drag-force measurements were taken on a modified prolate spheroid free of support interference in the 13-in. MSBS. This shape was one of two bodies tested in an effort to determine the drag-force measuring capabilities of the 13-in. MSBS. Results from tests of the other body are reported in Ref. 6. In addition, drag measurements were taken in the presence of a dummy sting to quantify support interference for the modified prolate spheroid at zero incidence.

Description of 13-in. Magnetic Suspension and Balance System

Figure 1a shows a sketch of the 13-in. system. For this system, motion is controlled in five degrees of freedom with no provision for generation of controlled magnetic roll torque on the model. Figure 1b shows a photograph of the system. This system has four electromagnets, arranged in a "V" configuration above the wind-tunnel test section, which provide the lift force, pitching moment, side force, and yawing moment. The 13-in. MSBS has a lift-force capability of about 6 lb depending on the size and shape of the iron core in the model. The drag electromagnet opposes the drag force. The test section passes through the drag electromagnet.

The control system is completely digitized with a PDP 11-73 minicomputer handling all of the control functions.[9] Bipolar thyristor power amplifiers supply the electromagnets. Feedback control of these amplifiers is used to stabilize the position and attitude of the model. Typical feedback loop repetition rates for this system are on the order of 256 cps. This control system receives position signals from an optical-position sensing system based on solid-state linear photodiode arrays. Laser-light sheets are directed across the test section to illuminate the arrays. The model position and attitude are inferred by locating the shadow of the model on the arrays. This technique is very geometry dependent. Abrupt changes in shadow positions are generally not tolerated by the control system; therefore, it is difficult to suspend many nonaxisymmetric shapes, especially bodies with wings at various pitch and/or yaw angles. Reference 10 gives more details on this optical position sensing system.

Description of Wind Tunnel

A small, low-speed ($M \leq 0.5$) wind tunnel was adapted to use with the 13-in. MSBS. As shown in Fig. 2, the tunnel is an

Presented as Paper 89-0648 at the AIAA 27th Aerospace Sciences Meeting, Reno, NV, Jan. 9-12, 1989; received April 22, 1989; revision received Nov. 22, 1989.

*Aerospace Engineer. Member AIAA.

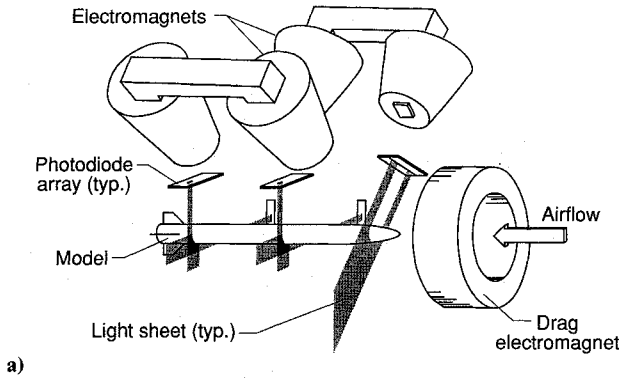

a)

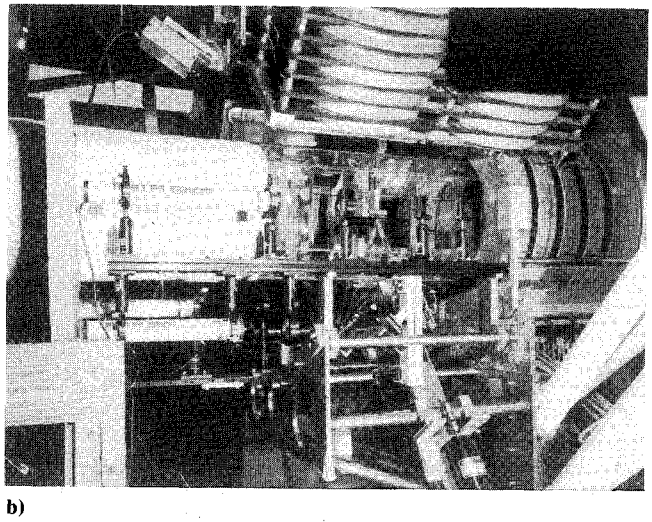

b)

Fig. 1 Sketch and photograph of 13-in. MSBS.

open-circuit design with air drawn into the tunnel from outside the building through a large bellmouth protected from outside contaminants by a screen enclosure. Constant diameter ducting extends the circuit to the first turn. Following the first turn, a quick diffuser and settling chamber with screens and honeycomb prepare the flow for entry into the contraction and test section. The contraction ratio is 8.43. The clear lexan test section is a modified octagon shape with major and minor axes of 12.56 and 10.68 in., respectively (Fig. 3). Reference 11 gives full details on the tunnel layout and calibration.

The flow quality in the tunnel is as follows: 1) a maximum deviation of $\pm 0.25\%$ in dynamic pressure across the test section, 2) velocity fluctuations in the streamwise direction of $0.2\% \pm 0.1$ for the Reynolds number range from 2×10^5/ft to 2×10^6/ft and, 3) flow angularity in pitch of about -0.5 deg relative to the cathetometer's reference. (The cathetometer is a remote fixed optical device used to measure relative vertical and horizontal displacements.)

Description of Model

Figure 4 shows a photograph of the model of the modified prolate spheroid ($L/d = 7.5$) used for this study. The modification involves the shaping of the front half of the model to provide a more favorable pressure gradient over this portion of the body.[12] The result of this modification is that the front half of the model is generally thinner than the rear half, which is half of a 7.5:1 prolate spheroid. The coordinates for the front half of the model are given in Ref. 13. The model is 12 in. long with a maximum diameter of 1.6 in. The model, which weighs about 1.7 lb, was made in two longitudinal halves using a fiberglass skin, which is foam filled around an embedded soft iron core. This ultralow carbon iron core is magnetized by the applied magnetic fields. The core is 1 in. in diameter by 6 in. long and is centered in the model.

A model of this shape was tested in the NASA Ames 12-ft pressure tunnel[12] to determine its boundary-layer transition characteristics. Results from these tests consisted of wake drag measurements and boundary-layer transition locations for various Mach numbers and Reynolds numbers. The last 5% of the Ames model was modified and faired into a sting used to support the model.

Another model of this shape was also recently tested in the Southampton University Magnetic Suspension and Balance System (SUMSBS).[14] The SUMSBS model, which is 7.25 in. long, is made of aluminum with the core made up of samarium-cobalt permanent magnets. These tests were aimed at checking out the very low drag coefficients reported in Ref. 12. In addition, drag measurements on this shape are currently of interest to researchers involved in computational design procedures for fuselage body shaping for minimum drag.[15] These researchers are hoping to reduce the drag of aircraft by increasing the extent of natural laminar flow on fuselages.

Description of Oil Flow Visualization Technique

A pigmented oil surface flow visualization technique was used to determine separation locations. This is a type of oil flow that uses a mixture of titanium dioxide (TiO_2) suspended in refined mineral oil. A small amount of oleic acid is added as an anticoagulant. The mixture was brushed on to the black model surface. The model was placed in the tunnel and suspended. The tunnel was then brought to test conditions, and, after the excess oil is wiped off, the TiO_2 was left deposited on the surface.

Data Corrections

Three-dimensional buoyancy corrections due to a longitudinal static pressure gradient in the test section were applied to this drag-force data using the technique outlined in Ref. 16. The body shape factor term $\lambda = 5.5$ used in these corrections was calculated using the potential solution plus boundary-

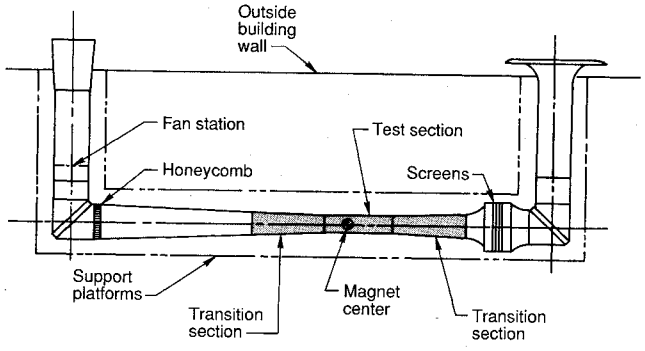

Fig. 2 13-in MSBS wind-tunnel layout.

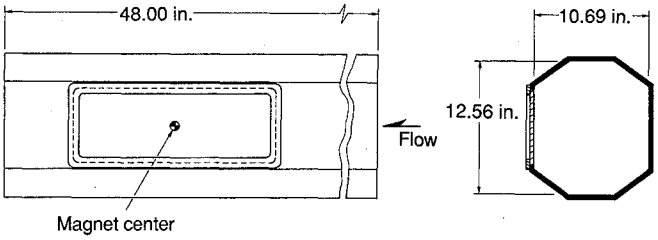

Fig. 3 Sketch of 13-in. MSBS wind-tunnel test section.

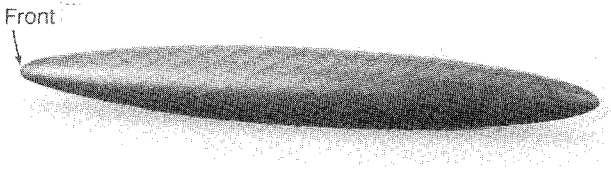

Fig. 4 Photograph of model.

layer results from the computer program SANDRAG.[17] For the tests with the dummy sting, the same body-shape factor was used. These buoyancy corrections are rather large, primarily due to the low drag forces (from about 1 g up to 30 g for these tests) present on this modified prolate spheroid. The drag coefficients corrected for buoyancy are reduced by 12 to 19% depending on the tunnel speed.

Both solid and wake blockage corrections were applied to the results of this study using the technique outlined in Ref. 18. The drag coefficients corrected for blockage are reduced by 2%.

Further details on the data reduction and corrections are given in Ref. 6.

Discussion of Experimental Results

Drag-Force Calibration

The calibration was performed using the setup shown in Fig. 5. Electromagnet current measurements were recorded as the model was loaded from 5.0 to 162.5 g. Current measurements were also recorded as the model was unloaded to check for hysteresis. The results from this calibration, shown in Fig. 6, indicate that there is no significant hysteresis in this data. The data was fitted with a second-order polynomial.

Drag-Force Characteristics and Repeatability of Data

Wind-on, drag-force measurements were taken for this body over the Mach number range from approximately 0.06 to 0.26. The results from run 1, presented in Fig. 7, show that $C_{D,\text{wet}}$ varies in an irregular manner over most of the Reynolds number range. This is the result of the data averaging scheme used during this portion of the tests. Not enough samples were used to determine the drag electromagnet current for each data point. This fact combined with the very low drag forces (from approximately 1 g at the lowest Reynolds number up to 30.5 g at the highest Reynolds number) leads to the irregular drag coefficient trend for run 1 in Fig. 7.

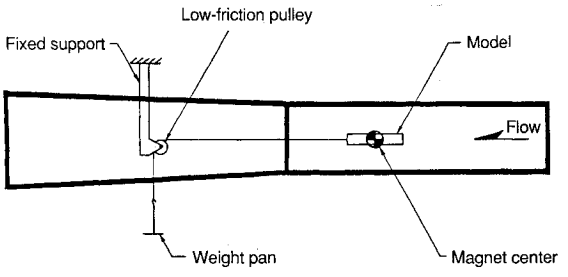

Fig. 5 Sketch of drag-calibration setup.

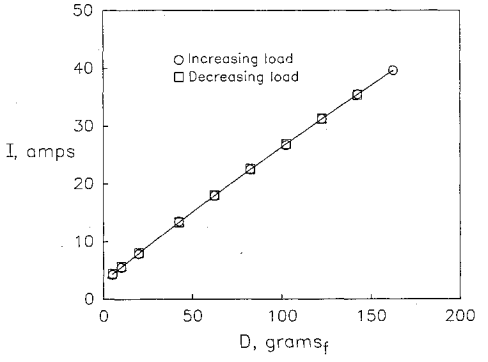

Fig. 6 Drag-force calibration.

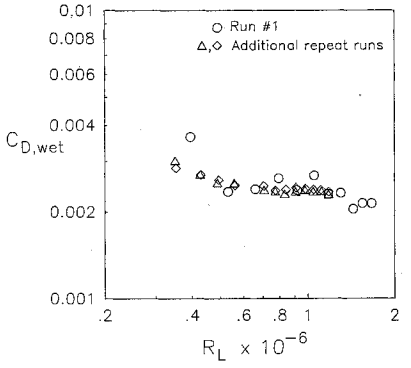

Fig. 7 Drag characteristics of modified prolate spheroid.

During the sting interference portion of these tests, two repeat runs were made using an updated averaging scheme based on an increased number of data samples. The results from these repeat runs are also shown in Fig. 7. The data trend is much smoother and consistent through the Reynolds number range. In addition, the repeatability of the data is quite good from one run to the next.

Comparison with Other Free Transition Data

This shape was also tested in the SUMSBS.[14] Run 1 from the present study is compared with the data from Ref. 14 in Fig. 8 (run 1 is used in Fig. 8 because it covers a larger Reynolds number range than the repeat runs from Fig. 7). The SUMSBS data have not been corrected for blockage and buoyancy; however, the blockage correction for $C_{D,\text{wet}}$ is estimated to be approximately 3%, and the buoyancy correction should be minimal since the test section was designed with a longitudinal divergence to avoid static pressure gradients. The drag coefficients from Ref. 14 are generally slightly higher than those from the present study. Correcting the SUMSBS data for blockage would lower the drag coefficients slightly and bring them more closely in line with the coefficients from the present study.

Data from tests of this shape (sting mounted) in the NASA Ames 12-ft pressure tunnel[12] are also shown in Fig. 8. These have been corrected for blockage. For the present study, the desire was to test the model in the 13-in. MSBS up to $M=0.5$ to overlap the lowest Reynolds number data from Ref. 12. However, static aerodynamic stability problems exhibited by the model would not allow testing above $M=0.26$. As a result, none of the data points from this study overlap those from

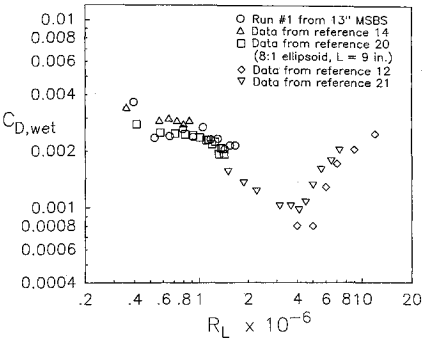

Fig. 8 Comparison of drag characteristics with data from other sources.

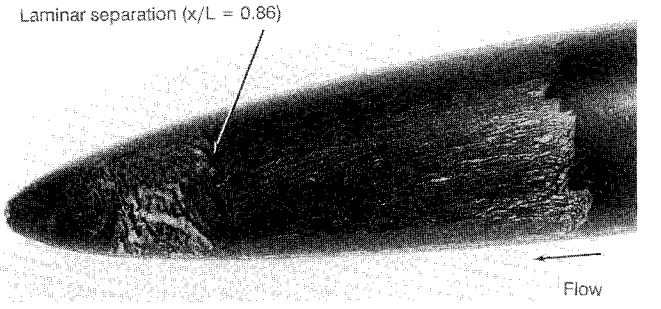

Fig. 9 Photograph of oil flow visualization, free transition; $R_L = 1.4 \times 10^6$.

Ref. 12. However, the two data sets are compared by looking at the drag coefficient trends and magnitudes shown in Fig. 8. [Note that the data shown in Fig. 8 from Ref. 12 was obtained from a crossplot of Fig. 11 (in Ref. 12) at a constant $M=0.1$.]

Reference 19 is used as a guide in this comparison. In this reference, Hoerner[19] shows the general trends of drag coefficient vs Reynolds numbers for streamlined bodies of revolution (see Fig. 22, Ref. 19). In the Reynolds number region from 10^4 to 10^5, Hoerner has estimated the drag coefficient assuming there is laminar boundary-layer separation without reattachment, as in the case of flow over a spheroid. From $R=10^5$ to 10^6, $C_{D,\text{wet}}$ decreases drastically because of the onset of transition and turbulent flow. The turbulent flow energizes the boundary layer and carries the flow farther around the body, resulting in a smaller wake and thus a lower drag coefficient than is present with laminar separation. From $R=10^5$ to $\sim 10^7$, transition is moving forward. At $\sim R=10^7$, there is fully turbulent flow over the bodies. The data from the present study follow the same trend as shown in the figure in Ref. 19. In particular, the drag data from this study slowly decrease over the entire Reynolds number range tested. This trend is very similar to the data trend shown by Hoerner for Reynolds numbers from 10^4 to 10^5. This slow decrease in $C_{D,\text{wet}}$ is typical of streamlined bodies with laminar separation in which the separation point moves slowly rearward with increasing Reynolds number. An example of this laminar separation is shown in Fig. 9, which is an oil-flow photograph from the present study showing laminar separation at $R_L=1.4\times 10^6$. In addition, the NASA Ames data shown in Fig. 8 exhibit an increase in drag coefficient associated with transition moving forward on the body. This trend is similar to the data trend shown by Hoerner for Reynolds numbers from 10^6 to 10^7.

Finally, two different sets of data on 8:1 ellipsoids are also included in Fig. 8 for comparison. These ellipsoids are slightly different from the shape used for the present study. In particular, they both have a slightly higher L/d (8 as compared to 7.5), and the front halves of these ellipsoids are not modified as in the case of the model from this study. These minor differences have little effect on the drag coefficients as shown in Fig. 8 where the ellipsoid data at the lower Reynolds numbers[20] is very close to the data from the present study. Figure 22 from Ref. 19 supports this result by showing that there are small differences in the drag coefficients for small changes in L/d at the higher L/d ratios (≥ 5) for R_L values from 4×10^5 to 1.2×10^6. The ellipsoid data from Ref. 20, which have been corrected for solid blockage, were obtained free of support interference in an MSBS at the Massachusetts Institute of Technology Aerophysics Lab.

The second set of 8:1 ellipsoid data is from Ref. 21 and it covers the R_L range from 1.5 to 7.3×10^6. These data have not been corrected for blockage and buoyancy; however, the blockage correction is estimated to be less than 1%. The last 7% of this ellipsoid was modified and faired into a sting used to support the model. The drag coefficients for this ellipsoid at approximately $R_L=1.5\times 10^6$ are low relative to both the other 8:1 ellipsoid data and to the data from the present study. On the other hand, these data generally agree well with the NASA Ames data except for a shift in the Reynolds number where transition first appears on the body. This shift is usually a function of the tunnel turbulence level. As in the case of the sting-mounted NASA Ames model, the drag on this ellipsoid was obtained by surveying pressures in the wake at the tail of the body. In both of these cases, the drag coefficients are low because this wake drag excludes the contribution from the base of a sting-mounted model. In addition, the presence of the sting can cause a reduction in the drag coefficient. This point will be discussed in detail in a later section.

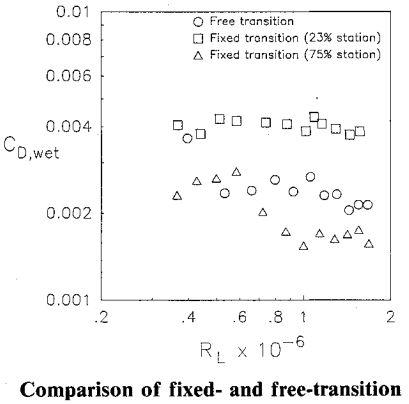

Fig. 10 Comparison of fixed- and free-transition data.

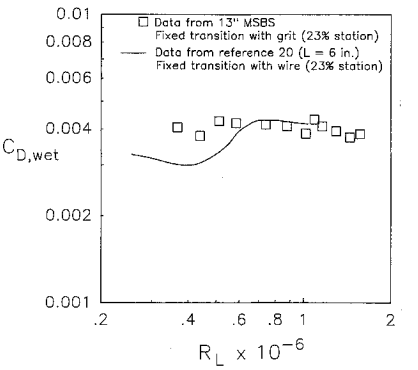

Fig. 11 Fixed-transition comparison.

Comparison of Free and Fixed Transition

Two fixed-transition runs were performed in an effort to assess the effect of fixing transition on laminar separation. Transition was fixed at two different locations using a single trip size. Three-dimensional abrasive grain transition grit was used with transition fixed at the 23 and 75% stations. The trip size used was grit number 60, which corresponds to a nominal trip size of 0.012 in. The transition grit was sized based on the size of a trip wire used on an 8:1 ellipsoid ($L=6$ in.) in Ref. 20.

Figure 10 shows a free- and fixed-transition comparison. All of the fixed-transition, drag-force data were taken using the original data averaging scheme. Fixing transition at the 23% station significantly increased the drag coefficients. The fairly constant $C_{D,\text{wet}}$ values with Reynolds number suggest that the boundary layer is fully turbulent beyond the grit through the entire Reynolds number range. Fixing transition this close to the nose resulted in turbulent flow over about 75% of the body. The contribution of this turbulent flow to the overall drag far outweighs the contribution from the small laminar separation region present in the free-transition case.

Fixing transition at the 75% station (ahead of the point of laminar separation) generally decreased the drag coefficients relative to the free-transition case. At Reynolds numbers up to 6×10^5, the boundary layer is thicker than the grit and it has no effect on tripping the boundary layer. However, as R_L increases up to 1×10^6, $C_{D,\text{wet}}$ decreases drastically. This is a transitional region where the boundary layer is not yet fully turbulent beyond the grit. However, there is enough energy imparted from the grit to keep the boundary layer attached beyond the original laminar separation point. Rearward movement of the separation point results in a lower $C_{D,\text{wet}}$. At $R_L=1\times 10^6$, the boundary layer is fully turbulent beyond the grit, and the drag coefficient remains fairly constant through the remainder of the Reynolds number range. These lower drag coefficients relative to the free-transition case are the result of having attached turbulent flow in place of the separated region at the tail of the model.

Comparison with Other Fixed-Transition Data

Figure 11 shows a comparison between the fixed-transition data at the 23% station from Fig. 10 and fixed-transition data

on an 8:1 ellipsoid from Ref. 20. In Ref. 20, the data are presented as a faired curve, which has been reproduced in Fig. 11. The tripping device used in the present study was a three-dimensional grit, whereas the ellipsoid was fitted with a single loop of wire. Both tripping devices were located at the same station on the models. Scaling of the wire diameter resulted in a required grit height of 0.011 in. The nominal trip size of 0.012 in. for the number 60 grit was slightly higher than the required height.

The grit appears to have fully tripped the boundary layer through the entire R_L range. However, the wire does not fully trip the boundary layer until approximately $R_L = 7 \times 10^5$. For higher Reynolds numbers, the two data sets are in good agreement. It is unclear why this transition to fully turbulent flow occurs at different Reynolds numbers for the two data sets. One possible explanation is given in Ref. 22. This reference states

> the two-dimensional roughness [wire] is more critical than the three-dimensional [grit] because it introduces larger disturbances. But, because the two-dimensional element produces two-dimensional disturbances, which must evolve into three-dimensional vortices before producing turbulence, the rate of movement of transition forward is less for the two-dimensional elements.

This delay in the forward movement of transition when using wire as a tripping device would account for the trend shown in Fig. 11.

Sting Interference

Tests were made with a dummy sting to quantify the effect of the sting's presence on the drag coefficients. These data were taken using the updated data averaging scheme mentioned earlier. Recall that additional runs using the original prolate spheroid, without modifications to accommodate the sting, were also made for comparison purposes.

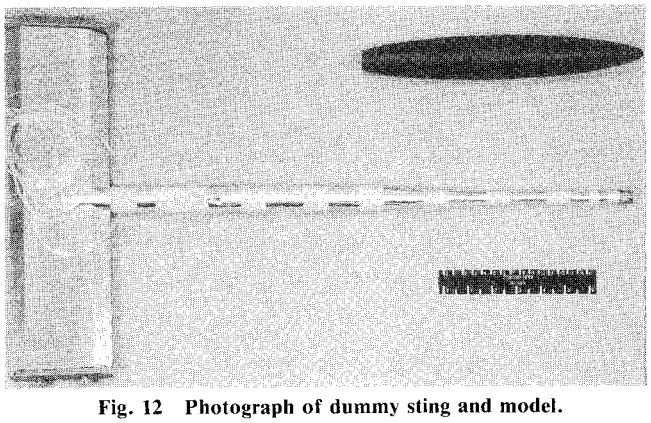

Fig. 12 Photograph of dummy sting and model.

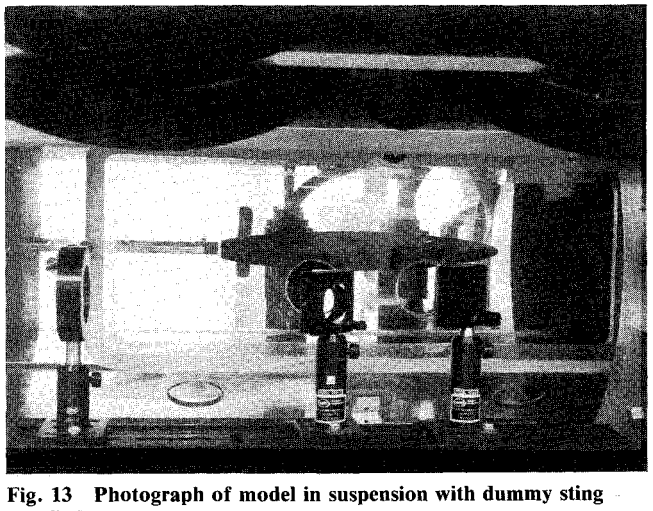

Fig. 13 Photograph of model in suspension with dummy sting installed.

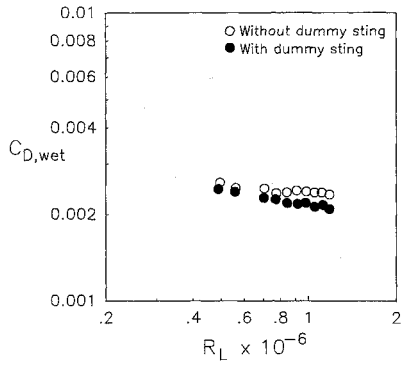

Fig. 14 Comparison of drag characteristics with and without dummy sting.

For the tests with the dummy sting, the model was shortened by cutting off the last 0.63 in. from the model's tail. A 0.60-in.-diam hole was drilled in the base of the model to accommodate the sting. A piece of very thin copper tape was attached to the walls of this hole as part of a fouling circuit used to indicate contact between the model and sting. During a data run, the model was actually "flown" on the sting without contact between them. A gap of approximately 0.04 in. was present between the sting and model, and the sting extended up into the model approximately 1/16 of an inch.

The sting, shown in Fig. 12, is 23.27 in. long and is attached to a vertical strut. The rear portion of the sting is 1 in. in diameter and 12 in. long. The front portion is nominally 0.5 in. in diameter and 6.5 in. long. A 4.77-in.-long flaired piece (3-deg half angle) joins the front and rear portions of the sting. In addition, a part of the fouling circuit is installed at the tip of the sting. As a result, the tip is approximately 0.53 in. in diameter. Fouling was not a problem during these tests.

Figure 13 is a photograph of the model in suspension prior to backing it over the dummy sting. Figure 14 is a comparison of the drag coefficients with and without the dummy sting. The reference area and model length for the original prolate spheroid were used for both data sets. The drag coefficients are lower for the case with the dummy sting. These lower coefficients may be attributable to one or both of the following:

1) The sting is acting as an extension of the body resulting in a higher fineness ratio shape that would reduce the drag coefficient (see Fig. 22, Ref. 19).

2) The sting is altering and possibly "breaking up" the separated wake region at the tail of the model.

In addition, note that model cavity pressures were not measured; consequently, a cavity pressure correction was not applied. Also, the data were not corrected for buoyancy due to the presence of the sting in the test section.

Also notice that the difference between the two data sets gets larger with increasing Reynolds number. For the first few data points, the difference is approximately 5%, whereas at the higher Reynolds numbers the difference is approximately 10%. It is believed that this gradual increase in the effect of the sting on the data is related to the slow rearward movement of the laminar separation point with increasing Reynolds number. In particular, as this separation point moves rearward, the downstream wake decreases in size, and the sting may have an increasing effect on altering this wake.

Conclusions

The primary objective of these tests was met by determining the drag-force measuring capabilities of the 13-in. MSBS. The drag-force calibrations are repeatable with no significant hysteresis. Wind-on drag-force measurements show only fair repeatability when using the original data-averaging scheme;

however, the use of an updated averaging scheme resulted in very good repeatability.

Comparisons of the drag-coefficient data with data on both the same shape and a similar shape generally show very good agreement. Two exceptions are the comparisons with the data on sting-mounted models. In both of these cases, the drag forces were determined from pressure measurements in the wake at the tail of the bodies. These wake drag measurements are low relative to the measurements from the other studies primarily because they exclude the drag contribution from the base.

Tests with transition fixed near the nose show an increase in the drag coefficients, whereas fixing transition a short distance ahead of the laminar separation point shows a decrease in the drag coefficients.

Tests with a dummy sting show that the drag coefficients are lower with the sting present. Also, the differences between the drag coefficients with and without the sting get larger as the Reynolds number increases.

References

[1]Tuttle, M. H., and Gloss, B. B., "Support Interference of Wind Tunnel Models—A Selective Annotated Bibliography," NASA TM-81909, 1981 (corrected 1988).

[2]Tuttle, M. H., and Lawing, P. L., "Support Interference of Wind Tunnel Models—A Selective Annotated Bibliography," supplement to NASA TM-81909, 1984 (corrected 1988).

[3]Tournier, M., and Laurenceau, P., "Suspension Magnetique d'une Maquette en Soufflerie," *Recherche Aeronautique,* No. 59, 1957, pp. 21–26.

[4]Tuttle, M. H., Kilgore, R. A., and Boyden, R. P., "Magnetic Suspension and Balance Systems—A Selected, Annoted Bibliography," NASA TM-84661, 1983.

[5]Matthews, R. K., Brown, M. D., and Langford, J. M., "Description and Initial Operation of the AEDC Magnetic Model Suspension Facility: Hypersonic Wind Tunnel (E)," U.S. Air Force, Arnold Engineering Development Center TR-70-80, May 1970.

[6]Dress, D. A., "Drag Measurements on a Body of Revolution in Langley's 13″ Magnetic Suspension and Balance System," AIAA Paper 88-2010, May 1988.

[7]Alcorn, C. W., and Britcher, C. P., "An Experimental Investigation of the Aerodynamic Characteristics of Slanted Base Ogive Cylinders Using Magnetic Suspension Technology," AIAA Paper 88-2011, May 1988.

[8]Britcher, C. P., Alcorn, C. W., and Kilgore, W. A., "Subsonic Sting Interference on the Drag of a Family of Slanted-Base Ogive-Cylinders," AIAA Paper 89-2206, July 1989.

[9]Britcher, C. P., "User Guide for the Digital Control System of the NASA/Langley Research Center's 13-Inch Magnetic Suspension and Balance System," NASA CR-178210, 1987.

[10]Tcheng, P., and Schott, T. D., "A Five Component Electro-Optical Positioning System," International Congress on Instrumentation in Aerospace Simulation Facilities Paper 87-CH2449-7, 1987, pp. 322–333.

[11]Johnson, W. G., Jr., and Dress, D. A., "The 13-inch Magnetic Suspension and Balance System Wind Tunnel," NASA TM-4090, 1989.

[12]Boltz, F. W., Kenyon, G. C., and Allen, C. Q., "The Boundary-Layer Transition Characteristics of Two Bodies of Revolution, a Flat Plate, and an Unswept Wing in a Low-Turbulence Wind Tunnel," NASA TN-D-309, 1960.

[13]Dress, D. A., "Drag Measurements on a Modified Prolate Spheroid Using a Magnetic Suspension and Balance System," AIAA Paper 89-0648, Jan. 1989.

[14]Newcomb, A. W., "The Effect of Sting Interference at Low Speeds on the Drag Coefficient of an Ellipsoidal Body Using a Magnetic Suspension and Balance System," NASA CR-181611, 1988.

[15]Dodbele, S. S., van Dam, C. P., Vijgen, P. M. H. W., and Holmes, B. J., "Shaping of Airplane Fuselages for Minimum Drag," AIAA Paper 86-0316, Jan. 1986.

[16]Glauert, H., "Wind Tunnel Interference on Wings, Bodies and Airscrews," British Aeronautical Research Council, R&M No. 1566, 1933.

[17]Wolfe, W. P., and Oberkamph, W. L., "SANDRAG—A Computer Code for Predicting Drag of Bodies of Revolution at Zero Angle of Attack in Incompressible Flow," Sandia National Lab., Albuquerque, NM, SAND85-0515, April 1985.

[18]Garner, H. C., Rogers, E. W. E., Acum, W. E. A., and Maskell, E. C., "Subsonic Wind Tunnel Wall Corrections," AGARD-AG-109, 1966.

[19]Hoerner, S. F., *Fluid-Dynamic Drag,* Hoerner Fluid Dynamics, Brick Town, NJ, 1965.

[20]Judd, M., Vlajinac, M., and Covert, E. E., "Sting-Free Drag Measurements on Ellipsoidal Cylinders at Transition Reynolds Numbers," *Journal of Fluid Mechanics,* Vol. 48, Part 2, 1971, pp. 353–364.

[21]Groth, E. E., "Low Speed Wind Tunnel Measurements on a Body of Revolution of Fineness Ratio 8," Northrop Aircraft Rept. BLC-6, Aug. 1953.

[22]Smith, A. M. O., and Clutter, D. W., "The Smallest Height of Roughness Capable of Affecting Boundary-Layer Transition," *Journal of the Aero/Space Sciences,* Vol. 26, No. 4, 1959, pp. 229–245 and 256.